



ELSEVIER

Contents lists available at ScienceDirect

Nuclear Instruments and Methods in Physics Research A

journal homepage: www.elsevier.com/locate/nima

High density processing electronics for superconducting tunnel junction x-ray detector arrays

W.K. Warburton^{a,*}, J.T. Harris^a, S. Friedrich^b^a XIA LLC, 31057 Genstar Road, Hayward, CA 94544, USA^b Lawrence Livermore National Laboratory, Livermore, CA 94550, USA

ARTICLE INFO

Available online 11 February 2015

Keywords:

Superconducting tunnel junctions
 Pre-amplifier
 Spectrometry
 Detector electronics

ABSTRACT

Superconducting tunnel junctions (STJs) are excellent soft x-ray (100–2000 eV) detectors, particularly for synchrotron applications, because of their ability to obtain energy resolutions below 10 eV at count rates approaching 10 kcps. In order to achieve useful solid detection angles with these very small detectors, they are typically deployed in large arrays – currently with 100+ elements, but with 1000 elements being contemplated. In this paper we review a 5-year effort to develop compact, computer controlled low-noise processing electronics for STJ detector arrays, focusing on the major issues encountered and our solutions to them. Of particular interest are our preamplifier design, which can set the STJ operating points under computer control and achieve 2.7 eV energy resolution; our low noise power supply, which produces only 2 nV/√Hz noise at the preamplifier's critical cascode node; our digital processing card that digitizes and digitally processes 32 channels; and an STJ *I*-*V* curve scanning algorithm that computes noise as a function of offset voltage, allowing an optimum operating point to be easily selected. With 32 preamplifiers laid out on a custom 3U EuroCard, and the 32 channel digital card in a 3U PXI card format, electronics for a 128 channel array occupy only two small chassis, each the size of a National Instruments 5-slot PXI crate, and allow full array control with simple extensions of existing beam line data collection packages.

© 2015 Elsevier B.V. All rights reserved.

1. Introduction

Superconducting tunnel junctions (STJs) are being developed as x-ray detectors in the 100–2000 eV range for synchrotron applications because of their demonstrated capability for obtaining energy resolutions below 10 eV at count rates approaching 10 kcps [1–3]. Detector sizes, however, are restricted to dimensions of approximately 250 μm by 250 μm or less by the presence of Fiske mode resonances in their *I*-*V* curves, which become too closely spaced at larger dimensions to allow an acceptable bias point to be found [4]. Therefore, to achieve good detection efficiencies, they are generally deployed in arrays to achieve larger solid detection angles. Arrays of 100+ elements have been produced and arrays of 1000+ elements are being contemplated [5–7]. Experience with smaller arrays, of up to 32 elements, which mimics the experience with similar sized HPGe detector arrays 25 years ago [8], makes it clear that instrumenting these arrays using multiple copies of single channel processing electronics causes unacceptable operational difficulties for array sizes much in excess of 30 detectors. Achieving the promise of STJ detectors

therefore requires the development of processing electronics that can place detector setup, calibration, and data collection under computer control. This essentially replicates the history of producing digital data systems for HPGe detectors, except at much higher channel counts, with more stringent limitations on energy resolution, and for a detector type that requires a significantly more complex procedure to set its operating bias.

We have recently completed a 5-year effort to develop compact, computer controlled, low-noise processing electronics for STJ detector arrays that preserve the detectors' inherent energy resolution, make their use accessible to non-specialists, and interface with only minor modifications to the various data collection packages found at synchrotron beam lines. In the following sections we focus on the major issues and developments in the project as follows: **Section 2**: our preamplifier design, which sets STJ operating points under computer control and achieves ~2 eV energy resolution; **Section 3**: a novel method for identifying Fiske modes that allows automated bias point setting; **Section 4**: an ultra-low noise power supply that delivers 16 V to the preamplifier's critical cascode circuit with only 2 nV/√Hz noise; **Section 5**: the system preamplifier and digital processing cards; **Section 6**: control software; **Section 7**: system performance showing 2.7 eV resolution at 250 eV and conclusions.

* Corresponding author. Tel.: +1 510 401 5760; fax: +1 510 401 5761.

E-mail address: bill@xia.com (W.K. Warburton).

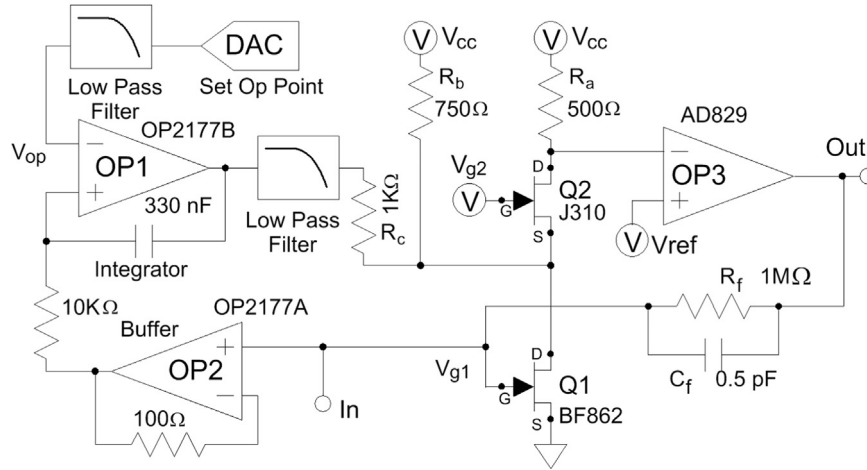


Fig. 1. Schematic of a single preamplifier channel.

2. Preamplifier design

A preamplifier optimized for STJ operation has several unusual requirements. First, it should be a transimpedance amplifier with a low input impedance at dc, since the STJ must be biased stably between Fiske mode resonances. Second, the preamplifier must be stable despite the STJ's relatively low dynamic resistance of $\sim 1\text{--}10\text{ k}\Omega$ and its relatively high capacitance of several nF. Third, STJ detectors are biased at a few hundred microVolts, but their bias points need to be individually determined and then held stably and reproducibly at the level of $1\text{ }\mu\text{V}$. For large arrays it is also a necessity that the bias determination process be computer controlled. Fourth, as the detectors output currents of order 100 nA/keV of x-ray energy and are capable of energy resolutions of a few eV, the preamplifier's input referred noise should be $1\text{ nV}/\sqrt{\text{Hz}}$ or less. Finally, the design should allow high density, relatively low cost scaling to large array sizes.

Fig. 1 shows a simplified schematic of our preamplifier design which adds ideas from Fabris et al. [9] to an earlier design by Friedrich et al. [10]. Its overall operations are as a two stage amplifier (the 1st stage being the Q2–Q3 cascode, the 2nd stage being OP3) with a feedback network comprising R_f and C_f . Changes in the STJ detector's current when it absorbs an x-ray are supplied through the $1\text{ M}\Omega$ feedback resistor R_f , for an output of $\sim 0.1\text{ V/keV}$. C_f stabilizes the feedback loop against the STJ detector's 2 nF capacitance.

In the Q1–Q2 FET cascode, the input transistor Q1 is the inexpensive, fairly high gain ($g_m=40$), and very low noise ($0.8\text{ nV}/\sqrt{\text{Hz}}$) BF862, which is operated close to its I_{DSS} value, with the current being supplied through 3 resistor legs— R_a , R_b , and R_c . The value of R_a is set by the desired first stage gain $G_1=g_m R_a$, where g_m is transistor Q1's transimpedance. With the voltage at Q1's drain set by V_{g2} minus the gate–source voltage drop of Q2, R_b is chosen to supply the remainder of Q1's nominal $14\text{ mA } I_{DSS}$. The current difference between this nominal value and Q1's true I_{DSS} value, which varies on a part-by-part basis, is supplied through R_c .

A novel feature of the circuit is that the detector's bias point, which is in the microvolt range, is set by adjusting the gate–source voltage V_{g1} of Q1, where V_{g1} is controlled by the amount Q1's drain–source current differs from I_{DSS} , I_{DSS} being the current I_{ds} that flows when V_{g1} is zero. In our design, V_{g1} is set using the OP1–OP2 feedback loop. In this circuit OP2 buffers Q1's gate voltage V_{g1} ; OP1 compares that to a filtered DAC output value and integrates the difference, thus changing the current through R_c until V_{g1} matches the set point established by the DAC. Both the DAC voltage and OP1 outputs are heavily low pass filtered (order 1 s time constants), since any noise in the current through R_c appears as attenuated signal noise (see [9] for the analysis). The resulting circuit uses only

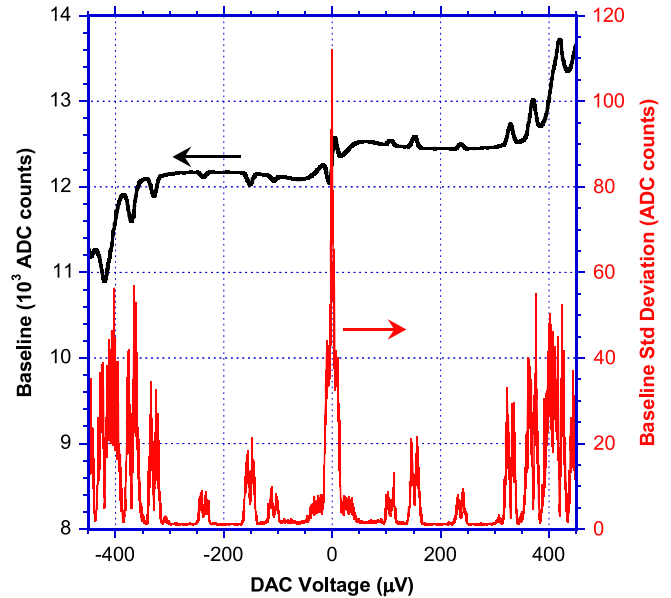


Fig. 2. Scans of STJ current and current noise versus bias voltage.

commercial grade surface mount parts and it thus both inexpensive and very compact, occupying only about 6 cm^2 of board space. Of critical importance, sweeping the DAC voltage across a range of STJ bias voltages allows both the STJ's characteristics to be determined and its bias point determined under full computer control.

3. Noise curves for finding Fiske modes

Because the STJ's current is supplied by OP3 through R_f , one can generate $I\text{--}V$ curves for the detector by recording V_{out} as a function of V_{DAC} . Fig. 2 shows a typical STJ $I\text{--}V$ trace (upper curve) generated this way. The small peaks are Fiske mode resonances in the STJ that are known to degrade energy resolution [11,12]. Because they are small, they are not well suited to machine identification processes of the sort required to automate the bias setting process.

Fiske modes are cavity oscillations in the STJs that increase the electronic noise in the external measuring circuit. See [11] and references therein for details. However, in working with the detectors, we realized that the same increase in electronic noise at a Fiske mode that damages resolution could also be used to identify its presence. Recalling that STJ detector current I_d is just

the preamplifier output voltage V_o/R_f , we therefore wrote a sub-routine that measured I_d several thousand times at each DAC setting and calculated the standard deviation from its mean (i.e. the electronic noise). Note that, since the units of voltage measurement are ADC units for an uncalibrated preamplifier output, the units of standard deviation are also ADC units. As shown in Fig. 2, plotting the standard deviation in the current I_d versus the DAC applied bias voltage makes even the smaller Fiske modes easy to identify and avoid in setting operating voltages.

To further characterize the correspondence between Fiske modes and energy resolution, we also made several measurements of the energy resolution at the 525 eV oxygen K line as we stepped V_{DAC} across a range of detector bias voltages. Results from one such experiment, Fig. 3, demonstrate the loss of detector energy resolution (upper curve) at Fiske mode resonances. We note that, while the standard deviations in the individual resolution values, as reported by the fitting program, are typically smaller than the point sizes, systematic errors—resulting from fluctuations in the data collected and from the selected fitting regions—are larger than this, as seen in the point-to-point scatter. This scatter is small, compared to the losses in resolution seen as the operating point crosses over a Fiske mode. Good operating points are thus found to lie in any flat area

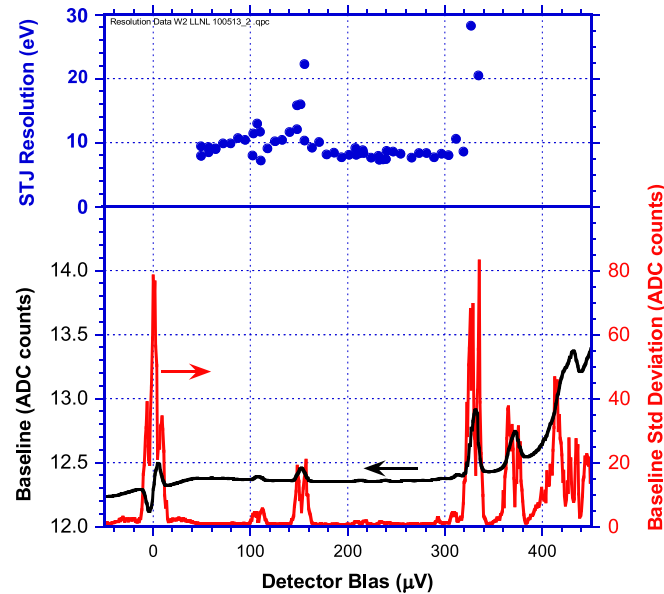


Fig. 3. STJ I - V and noise- V scans and associated STJ energy resolutions.

between the Fiske modes, and the good signal-to-noise seen in the Noise vs V_{DAC} curve (lower trace) greatly simplifies the process of identifying these good operating regions and thus biasing a detector array with a large number of channels under full computer control.

4. Ultra-low noise power supply

While the cascode in Fig. 1 provides excellent energy resolution, it is also sensitive to noise v_{nc} in supply voltage V_{cc} , since any change in V_{cc} appears directly at the input of OP3 with an input-referred value v_{nc}/G_1 . Since our design calls for a total input referred noise of order $1 \text{ nV}/\sqrt{\text{Hz}}$, v_{nc} should be no more than $2\text{--}3 \text{ nV}/\sqrt{\text{Hz}}$ to not contribute significantly. Traditionally, STJ preamplifiers have been battery operated for this reason, but that solution does not scale well to 100's of detectors operating for long periods of time.

We therefore developed a novel ultra-low noise power supply whose schematic is shown in Fig. 4. The supply has two stages, one active, and one passive. In both cases the stage output voltage is compared to a heavily filtered reference voltage and fed back to a control transistor. Eq. 1a and b shows the dominant noise terms for the two stages, where A is the OpAmp gain, $g_{be}=20$ and $g_{ce}=1/900$ are transconductances of the 2SCR543D transistor, and v_{nRb} is its base resistor (0.16Ω) noise. The output noise of the first stage is essentially the input referred noise of OP1 in parallel with 100Ω , so that the output noise of the second stage is then dominated by the base resistor noise.

$$\begin{aligned}
 a: \quad v_{nout1} &= v_{nA} + (v_{nin}g_{ce})/(Ag_{be}) \\
 b: \quad v_{nout2} &= v_{nRb} + (v_{nout1}g_{ce})/g_{be}
 \end{aligned}
 \tag{1}$$

Noise at this level is difficult to measure. Following the methods of [13,14], we made a correlated noise measurement of the outputs of two low noise preamplifiers whose inputs were both connected to the supply output. The basic concept here is that, while each preamplifier will add its own noise to the measurement of the input voltage, the noise of the two preamplifiers is not correlated and can be removed by measuring only the correlated component of their outputs and averaging over a long period of time to suppress random fluctuations.

Fig. 5 shows the power supply's noise spectrum, thus measured. In order to calibrate this result, we used the same system to measure a noise spectrum with its input grounded as well as attached to either a 62Ω or a 243Ω metal film resistor. These resistors are known from electronic theory to generate Johnson–Nyquist thermal noise with a white spectral density of 1 and $2 \text{ nV}/\sqrt{\text{Hz}}$, respectively. While there is some correlated pickup noise in the measurements (the low frequency spikes) these results show that the supply

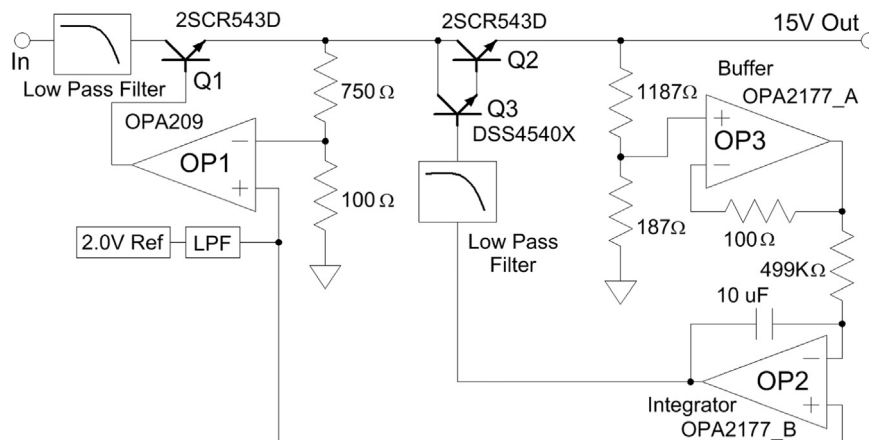


Fig. 4. Schematic of the $2 \text{ nV}/\sqrt{\text{Hz}}$ ultra-low noise power supply.

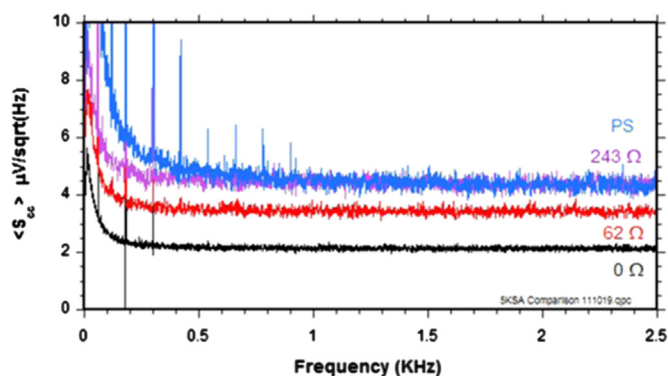


Fig. 5. Noise spectrum of the ultra-low noise power supply compared to the noise spectra of two resistors: 62 Ω (1 nV/ $\sqrt{\text{Hz}}$) and 243 Ω (2 nV/ $\sqrt{\text{Hz}}$).

achieves about 2 nV/ $\sqrt{\text{Hz}}$ down to 500 Hz while delivering 0.5 A. We can therefore expect a negligible contribution to our preamplifier's input referred noise from V_{CC} .

5. System preamplifier and digital processing cards

For purposes of noise control and modularity, the complete processing chain was divided between two cards, an analog preamplifier card and a digital filtering and processing card. The only digital components on the analog card are a CPLD for command processing and the DACs used to set the STJ detector bias values. Both the DAC command words and the Complex Programmable Logic Device (CPLD) clock are supplied by the digital card and both are turned off during data collection, eliminating all fast digital signal level transitions that might otherwise contaminate the low noise STJ signals through ground loops or otherwise.

5.1. Preamplifier card

As shown in Fig. 6, the STJ preamplifier card is implemented in a Euro-card format and mounts 32 preamplifiers, 16 per side. 16 dual relays, visible along the horizontal center axis of the card, serve to isolate the STJ detectors during power-up. Two 16 channel DACs (top and bottom right hand corners of the card) set the preamplifiers' operating points and are digitally set by the DXP processor card

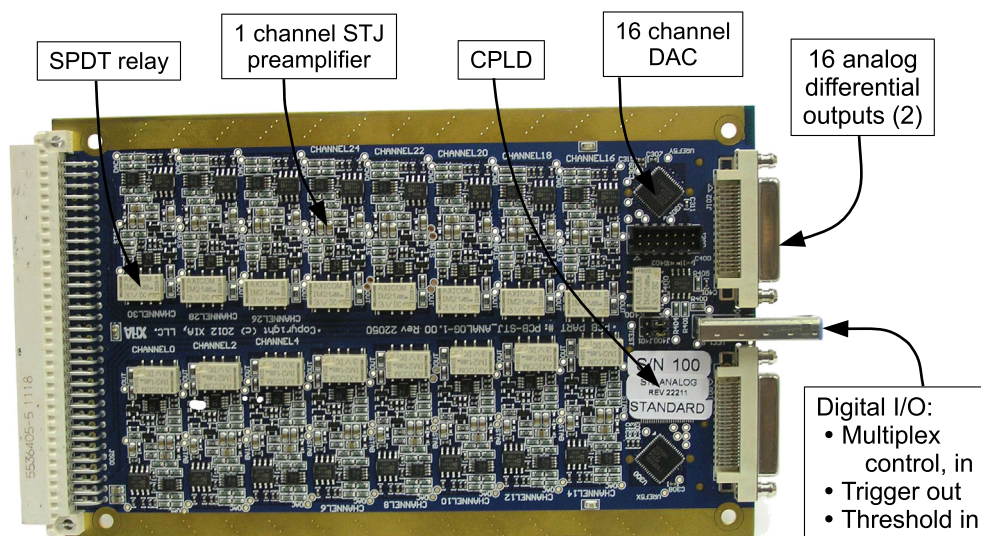


Fig. 6. 32 channel STJ preamplifier card in Euro-card format.

through a CPLD, using the middle connector. The card's output signals are differential, passing through 2 high density connectors (card's right edge, upper and lower) and twisted pair cables to the DXP card. The card receives both its power and input signals through the back plane connector (card left edge). The cascode power to each card is filtered separately by a power conditioning card in the preamplifier chassis using the circuit discussed in Section 4.

5.2. Digital processor card

Figs. 7 and 8 show a block diagram and an image of the digital processor card. The card was designed by modifying the front end of our standard XIA xMAP card, which is widely used with hard x-ray detector arrays at synchrotron facilities world-wide. The card therefore functionally appears as a "32 channel xMAP" and, except for its STJ-specific functions, can be fully controlled by existing xMAP software packages. This minimizes both facility integration effort and the new user's learning curve.

The card's front end comprises 4 analog sections, each containing 8 input buffers, followed by a Texas Instruments AFE5801 which contains a single VGA and eight channels of 12-bit, 65 MHz ADC. The AFE5801s connect in pairs to two FPGAs where digital processing detects signal pulses from the individual detectors, extracts their energies, checks for pile-up, and passes good values through the system FPGA to memory. Other standard XIA xMAP functions are also implemented, including trace capture, baseline correction, and ping-pong memory reading. A DSP handles special functions, including STJ noise scans. Standard PXI communication is implemented using a PLX chip. Direct back plane connections implement inter-card communications, allowing such features as coincidence detection to be provided in larger systems.

6. Control software

Because the STJ DXP card's back-end hardware and firmware were derived from XIA's 4 channel xMAP, we were able to use the xMAP interface and control program ProSpect to control this card as well, with only two significant modifications—gain matching and I - V trace capture. We therefore developed a new ProSpect gain matching panel that places 32 matched single line spectra in a lower block and their deviations from their mean in an upper block directly above. Working with an identified x-ray line with good statistics, gain

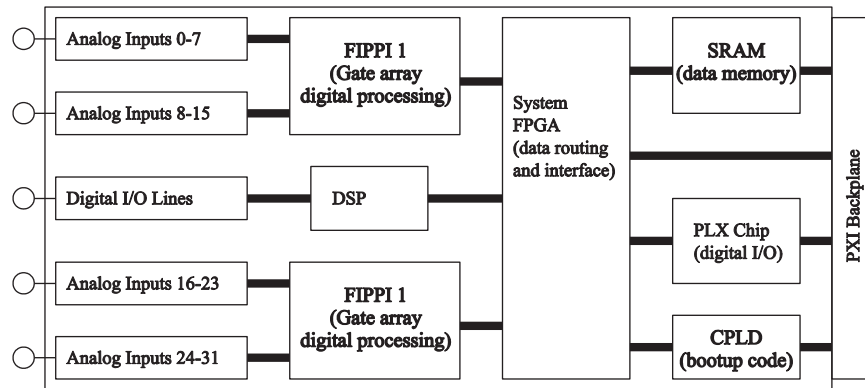


Fig. 7. Block diagram of 32 channel STJ digital processing card.

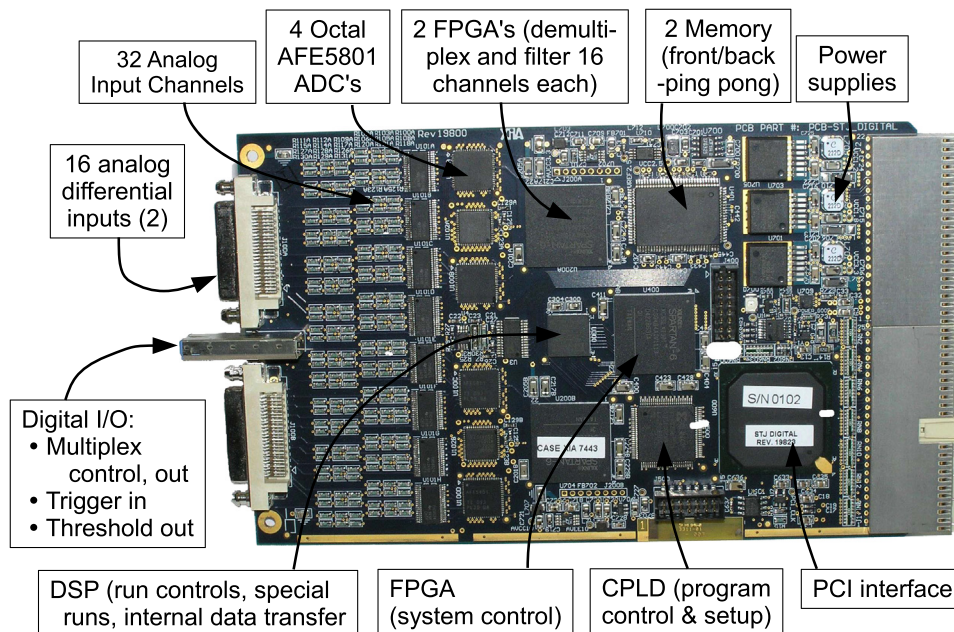


Fig. 8. 32 channel STJ digital processing card in PXI format.

matching is a two step process: first, for adjusting the average gains of the AFE5801's VGAs and then digitally making channel-by-channel fine corrections. After gain matching, channel variations from the mean are typically less than 0.2% (1 eV at 500 eV). This process takes the program a few iterations and the user can observe both its progress and conclusion in the gain matching panel.

We also developed a new ProSpect I - V control panel and associated data collection routine. Here the bias voltage applied to the STJ detectors is stepped across a preset range, where the starting offset, step size and number of steps are entered via the panel, and the resultant detector currents and their rms noise are captured at each step. While data on all detectors are taken simultaneously, at this point in our development, the detectors must still be examined individually to set their bias points. To make this process as simple and fast as possible, a pair of traces similar to those shown in Fig. 2 are plotted for each detector. First, the inversion point in the I - V curve, which occurs at 0V, is selected with a cursor and entered using a Zero Adjust button to calibrate the scan. The cursor is then moved to select the STJ's operating point, which is entered via the Set STJ Bias button. Both values are saved to memory to characterize the detector. After all the detectors have been biased, data collection proceeds as with an xMAP, using either ProSpect or any other convenient software package.

7. System performance and conclusions

The ultimate test of a low noise preamplifier is how well it performs with actual STJ detectors. Fig. 9 shows data collected from a $(208 \mu\text{m})^2$ Ta/Al/AlOx/Al/Ta STJ at the Advanced Light Source. In order to avoid line width contributions associated with molecular emission lines, we illuminated the detector directly with 250 eV synchrotron x-rays from a grating monochromator whose resolution was 0.2 eV. The collected spectrum shows the line at 250 eV and several higher order lines. The inset expands the 250 eV line, showing that the preamplifier achieves 2.7 eV resolution at an input counting rate of 230 cps using a digital trapezoidal filter with an 18 μs peaking time. This result demonstrates that, in most cases, energy resolution will not be limited by the electronics.

In this paper we have summarized our development of a set of high performance, low cost electronics for STJ x-ray detector arrays, focusing on the major issues encountered and our solutions to them. In particular, we developed a compact preamplifier based on a low cost FET that allows STJ operating points to be determined and set under digital control. Using this circuit we produced a card carrying 32 such circuits in a 3U EuroCard format. The preamplifier card's outputs are then processed using a 32 channel

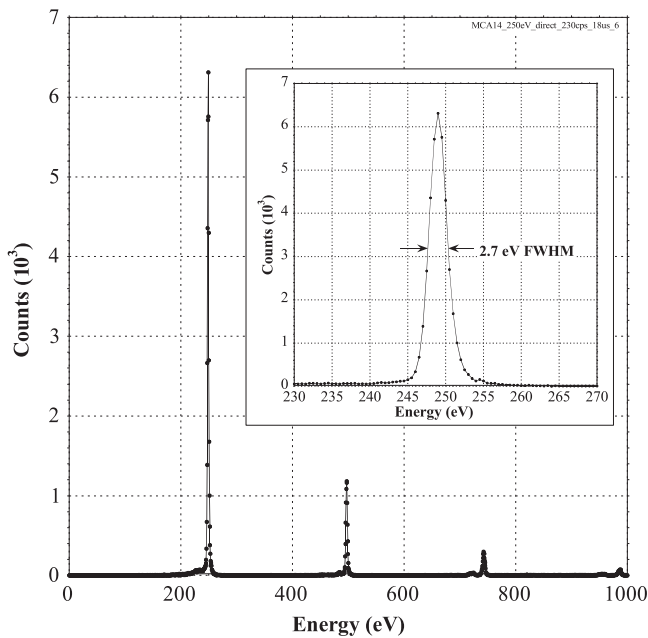


Fig. 9. STJ energy spectrum of x-ray lines from a soft x-ray monochromator. The inset expands the first line at 250 eV.

digital card in a 3U PXI format. By basing this card on XIA's popular xMAP design, we not only minimized development effort but also maximized software compatibility with beam line data collection software world-wide. To accommodate STJ-specific issues, we developed firmware routines to match gains across large numbers of detectors and to simplify the STJ bias setting procedure by measuring STJ noise-voltage curves under full computer control. The complete system was shown to attain an energy resolution of 2.7 eV FWHM at 250 eV, which is less than typical linewidths in the soft x-ray band. With an achieved density of 32 channels per

card for both the analog preamplifiers and the digital processing, electronics for a 128 channel array occupy only two small chassis, each the size of a National Instruments 5 slot PXI crate, while the xMAP-like interface allows array control with simple extensions of existing beam line data collection packages.

Acknowledgments

Major support for this work was provided by the US Department of Energy SBIR Program under Award No. DE-SC0002256. Part of this work was performed under the auspices of the U.S. DOE by LLNL under Contract DE-AC52-07NA27344.

References

- [1] M. Frank, et al., *Review Scientific Instruments* 69 (1998) 25.
- [2] P. Verhoeve, *Journal of Low Temperature Physics* 151 (2008) 675.
- [3] S. Friedrich, et al., *Journal of Low Temperature Physics* 167 (2012) 741.
- [4] M.H. Carpenter, et al., *IEEE Transactions on Applied Superconductivity* 23 (2013) 2400504.
- [5] S. Shiki, M. Ukibe, Y. Kitajima, M. Ohkubo, *Journal of Low Temperature Physics* 167 (2012) 748.
- [6] S. Friedrich, et al., *Journal of Low Temperature Physics* 176 (2014) 553.
- [7] G. Fujii, M. Ukibe, S. Shiki, M. Ohkubo, *Journal of Low Temperature Physics* 176 (2014) 255.
- [8] S.P. Cramer, O. Tench, M. Yocum, G.N. George, *Nuclear Instruments and Methods in Physics Research, Section A* 266 (1988) 586.
- [9] L. Fabris, N.W. Madden, H. Yaver, *Nuclear Instruments and Methods in Physics Research, Section A* 424 (1999) 545.
- [10] S. Friedrich, K. Segall, M.C. Gaidis, C.M. Wilson, D.E. Prober, *IEEE Transactions on Applied Superconductivity* 7 (1997) 3383.
- [11] S. Friedrich, M.F. Cunningham, M. Frank, S.E. Labov, A.T. Barfknecht, S.P. Cramer, *Nuclear Instruments and Methods in Physics Research, Section A* 444 (2000) 151.
- [12] S. Friedrich, M.H. Carpenter, O.B. Drury, W.K. Warburton, J. Harris, J. Hall, R. Cantor, *Journal of Low Temperature Physics* 167 (2012) 741.
- [13] C.K. Boggs, A.D. Doak F.L. Walls, Measurement of voltage noise in chemical batteries, in: *Proceedings of the IEEE International Frequency Control Symposium* (1995), pp. 367–373.
- [14] E. Rubiola and F. Vernotte, The cross-spectrum experimental method, (http://arxiv.org/PS_cache/arxiv/pdf/1003/1003.0113v1.pdf).